Journal of Applied Polymer Science

Nonisothermal Crystallization Kinetics of Poly(butylene terephthalate)/Multiwalled Carbon Nanotubes Nanocomposites Prepared by *in situ* Polymerization

Hui Fang, Fangjuan Wu
School of Materials Science and Engineering, Fujian University of Technology, Fuzhou 350118, China
Correspondence to: H. Fang (E-mail address: hfang79@163.com)

ABSTRACT: Poly(butylene terephthalate)/multiwalled carbon nanotubes (PBT/MWNT) nanocomposites were prepared by *in situ* ring-opening polymerization of cyclic butylene terephthalate oligomers (CBT). The nonisothermal crystallization behavior of the neat PBT and the PBT/MWNT nanocomposites was analyzed quantitatively. The results reveal that the combined Avrami/Ozawa equation exhibits great advantages in describing the nonisothermal crystallization of PBT and its nanocomposites. The presence of MWNTs has the nucleation effect promoting crystallization rate for the nanocomposites, and the maximum one is observed in the nanocomposite having 0.75 wt % MWNT content. On the other hand, the addition of MWNTs has the impeding effect reducing the chain mobility and retarding crystallization, which is confirmed by the crystallization activation energies. However, the nucleation effect of MWNTs plays the dominant role in the crystallization of PBT/MWNT nanocomposites, in other words, the incorporation of MWNTs is increasing the crystallization rate of the nanocomposites. © 2014 Wiley Periodicals, Inc. J. Appl. Polym. Sci. **2014**, *131*, 40849.

KEYWORDS: composites; crystallization; differential scanning calorimetry (DSC); polyesters; ring-opening polymerization

Received 16 December 2013; accepted 9 April 2014
DOI: 10.1002/app.40849

INTRODUCTION

Poly(butylene terephthalate) (PBT), a commercial engineering thermoplastics, exhibits various excellent properties including mechanical properties, rapid crystallization rate, chemical resistance and excellent moldability. These good properties make PBT widely used in thermoplastic matrix composites for gears, machine parts, small pump housings, and insulators.[1]

Of potential fillers for polymer composites, carbon nanotubes (CNTs) including both singlewalled and multiwalled ones (SWNTs and MWNTs) have aroused more and more attention on account of their unique mechanical, electrical, and thermal properties since the landmark paper in 1991 by Iijima[2] and have been widely used in fabrication polymer/CNT nanocomposites, including PBT/CNTs composites.[3–6] Nevertheless, the potential of CNTs as reinforcements for polymers has been limited because the homogeneous dispersion of CNTs and perfect interfacial adhesion between CNTs and polymer matrix in obtained nanocomposites are difficult to be realized.[7] To overcome this issue, several preparation methods are in use for combining polymers and CNTs into composite materials. These include functionalization,[8,9] intercalation,[10] electrochemical deposition,[11] latex technology,[12,13] electrospinning,[14,15] solution casting technique,[16] and *in situ* polymerization.[17–20]

In this work, PBT/MWNT nanocomposites were prepared by *in situ* method in the presence of cyclic butylene terephthalate oligomers (CBT), butyl tin chloride dihydroxide and functionalized multiwalled carbon nanotubes (f-MWNTs). CBT has the characteristics of water-like viscosity and ability to be rapidly polymerized to form PBT, which could favour the dispersion of nanotubes in matrix to some extent. In addition, f-MWNTs were prepared in our previous work.[21] A cyclic initiator containing Sn–O bonds was covalently attached to the MWNT surface. The Sn–O bond has been shown to be an active polymerization site for polymerization of lactones and cyclocarbonates according to coordination–insertion mechanism. In a word, based on the *in situ* ring-opening polymerization of CBT initiated by butyl tin chloride dihydroxide, as an initiator, and f-MWNTs, *in situ* polymerization and *in situ* compatibilization would take place during the preparation of PBT/MWNT nanocomposites.

Considering that PBT is a semicrystalline polymer, its mechanical and physical properties are governed by the supramolecular morphology, which is in turn controlled by the crystallization process. Therefore, as a part of a series of work[22] on the effect of MWNTs on the PBT/MWNT nanocomposites prepared by *in situ* method, the nonisothermal crystallization kinetics of PBT with MWNTs

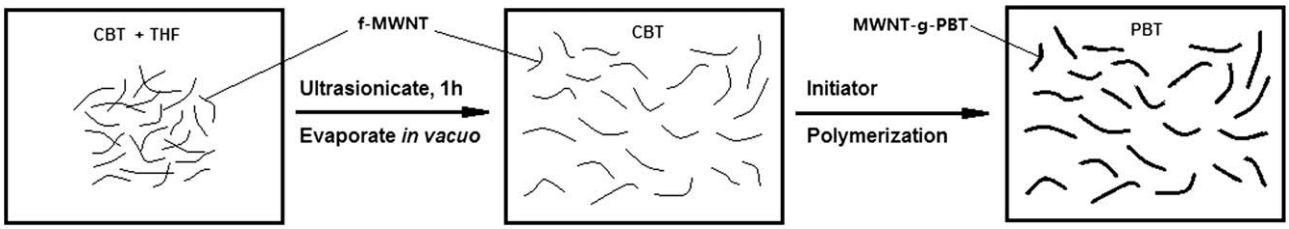

Scheme 1. Dispersion of MWNTs and preparation of PBT/MWNT nanocomposites.

was studied in the present contribution. Although the nonisothermal crystallization kinetics of PBT/MWNT nanocomposites has been examined,[23] to our knowledge no report has been found in literature regarding the effect of MWNTs on the PBT/MWNT nanocomposites obtained by *in situ* mothed. In this study, the crystallization kinetics of PBT/MWNT nanocomposites was investigated by differential scanning calorimetry (DSC). Several models were employed to analyze the nonisothermal crystallization data. The crystallization activation energies were investigated by the Kissinger method as well.

EXPERIMENTAL

Materials

CBT oligomers (CBT 100) and butyl tin chloride dihydroxide were purchased from Cyclics Corp. (New York). Tetrahydrofuran (THF) with analysis grade was provided by Shanghai Chemical Reagent Corp. (Shanghai, China) and f-MWNTs were prepared in previous work.[21]

Preparation of PBT/MWNT Nanocomposites

As shown in Scheme 1, the desired amount of f-MWNTs was added to a solution of 30 g of CBT and 150 mL of tetrahydrofuran (THF), and a stable suspension was obtained with the aid of ultrasonication for 1 h at room temperature. Most of the THF was evaporated *in vacuo* at 50°C, and then, the black mixture was heated to 200°C *in vacuo* for another 30 min to remove trace amount of THF. Afterward, appropriate amount of butyl tin chloride dihydroxide was added to ensure that the contents of the initiator in all preparations were identical. The whole procedure was completed within 30 min under mechanical stirring at a speed of 500 rpm. According to the content of the MWNTs (weight percentage), the nanocomposites were identified as PBT/MWNT-0.5, PBT/MWNT-0.75 and PBT/MWNT-1.0.

Separation of Homo-Poly(Butylene Terephthalate) (Homo-PBT)

The specimen of each PBT/MWNT nanocomposites was firstly extracted by THF to remove unreacted CBT, and then was dissolved in trifluoroacetic acid/trichloromethane (1:3, v/v) solvent mixture under stirring overnight at room temperature. After

Table I. M_v and *CBT%* Values of the Neat PBT and the PBT/MWNT Nanocomposites

Sample	M_v	*CBT%*
neat PBT	61,539	98.9%
PBT/MWNT-0.5	61,334	98.0%
PBT/MWNT-0.75	60,193	97.7%
PBT/MWNT-1.0	59,379	97.2%

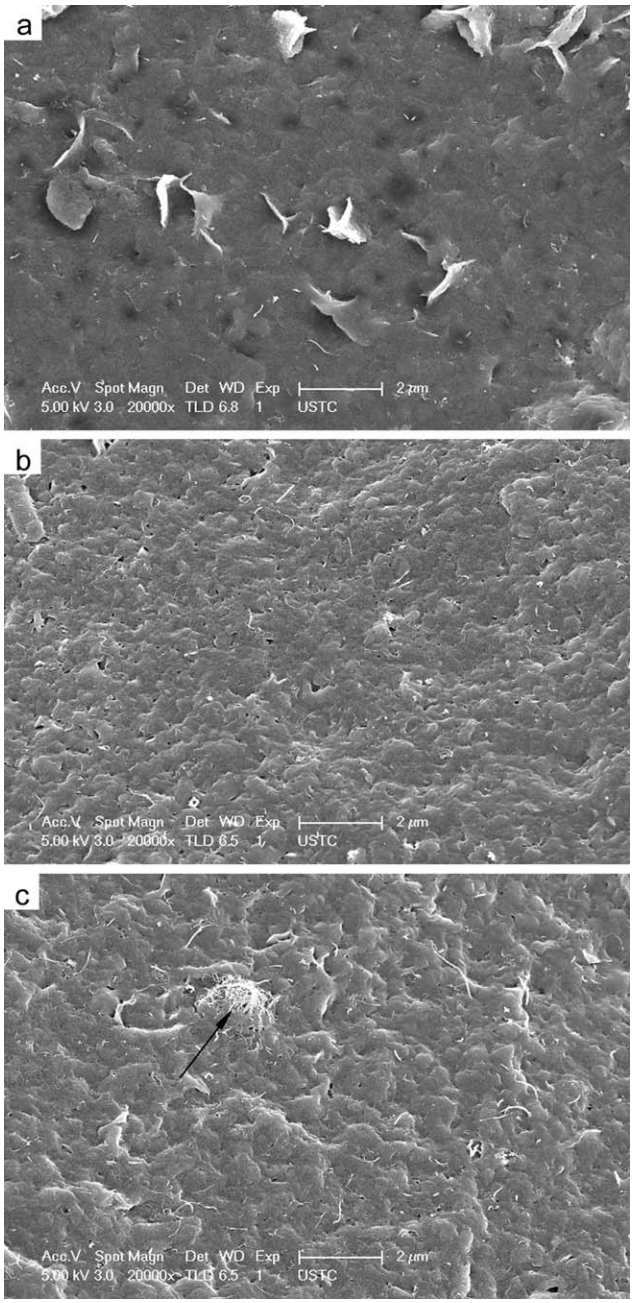

Figure 1. FESEM images of the fracture surface of (a) PBT/MWNT-0.5, (b) PBT/MWNT-0.75, and (c) PBT/MWNT-1.0.

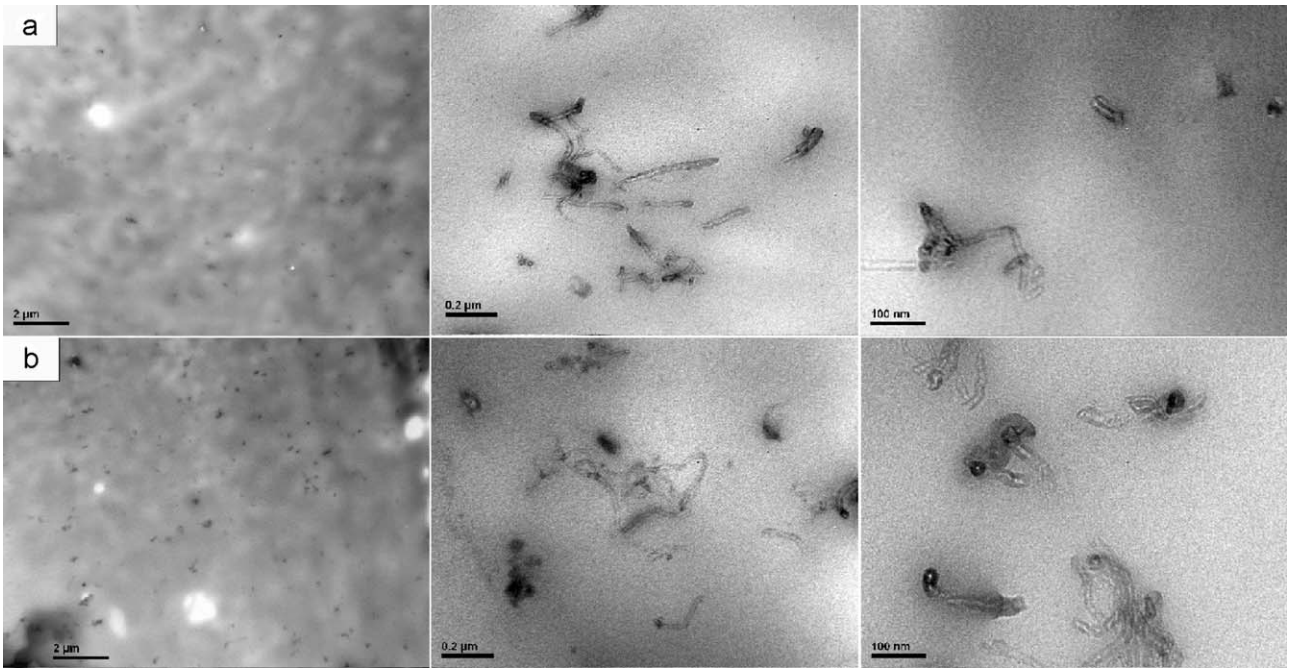

Figure 2. TEM images of (a) PBT/MWNT-0.5 and (b) PBT/MWNT-0.75 at different magnification.

this, the suspension was separated by filtration. The homo-poly(butylene terephthalate) (homo-PBT) was precipitated in excess methanol from the collected filter, washed thoroughly with methanol, and finally, dried *in vacuo* at 80°C for 24 h. The recovered polymer was prepared for viscosity measurement.

Characterization

To measure the conversion of CBT to PBT, a small amount specimen was extracted with THF to remove unreacted CBT, and then was dried in a vacuum oven at 80°C for 24 h. The CBT conversion (*CBT%*) was calculated by eq. (1):

$$CBT\% = \frac{m_1 - m_0 \times MWNT\%}{m_0 \times (1 - MWNT\%)} \times 100\% \quad (1)$$

where m_0 is the original mass of the specimen, m_1 the mass of the specimen after extracted and dried, and *MWNT%* the content of MWNTs in the nanocomposites.

The intrinsic viscosity ($[\eta]$) of the samples dissolved in 0.5 g/dL concentrated mixture solvent of phenol/1,1,2,2-tetrachloroethane (60:40, w/w) was determined with an Ubbelohde viscometer (Shanghai, China) thermostated at 30 ± 0.5°C in a water bath. The measurements were carried out at only one specific concentration according to the single-point method.[24] The values of $[\eta]$ for the PBT and the homo-PBT of the nanocomposites were calculated according to the following equation:[25]

$$[\eta] = \frac{\sqrt{2(\eta_{sp} - \ln \eta_{rel})}}{c} \quad (2)$$

where η_{sp} is the specific viscosity, η_{rel} the relactive viscosity and c the concentration. Meanwhile, M_v was obtained from the Mark–Houwink equation:[24]

$$[\eta] = 1.166 \times 10^{-4} M_v^{0.871} \quad (3)$$

The dispersion of MWNTs in the nanocomposites was observed by using field emission scanning electron microscopy (FESEM, JEOL 6700F) at an acceleration voltage of 5 kV. Because of the MWNTs embedded in the matrix, all of the cryogenically fractured surfaces were etched by NaOH/ethanol (10 wt %) to remove the polymer coating on the outside of the MWNTs.

Transmission electronic microscopy (TEM) was performed on a JEOL/JEM-200 CX at an acceleration voltage of 160 kV. Due to the obvious aggregation of MWNTs observed in the sample of PBT/MWNT-1.0 by FESEM, this sample was not investigated by TEM. The other samples were ultramicrotomed with a diamond knife on a Leica Ultracut UCT microtome at −60°C to obtain 60–80 nm thick sections.

Differential scanning calorimetry (DSC, Shelton CT) was used to record the nonisothermal crystallization of the neat PBT and the PBT/MWNT nanocomposites. All samples were weighted to be in the range 6–7 mg. For each measurement, the samples were first heated to 250°C at a heating rate of 10°C/min under nitrogen atmosphere, maintained at this temperature for 5 min to eliminate the previous thermal history. The nonisothermal crystallization kinetics was studied by cooling a sample from 250°C to 50°C at a rate of 5, 10, 20, 40°C/min, respectively.

RESULTS AND DISCUSSION

Viscosity-Average Molecular Weight (M_v) and CBT Conversion (*CBT%*)

To estimate the influence of the MWNTs on *in situ* polymerization of CBT, the M_v and the *CBT%* of all samples were investigated. As shown in Table I, the MWNTs had little influence on the values of M_v and *CBT%* of the resultant PBT in the case of

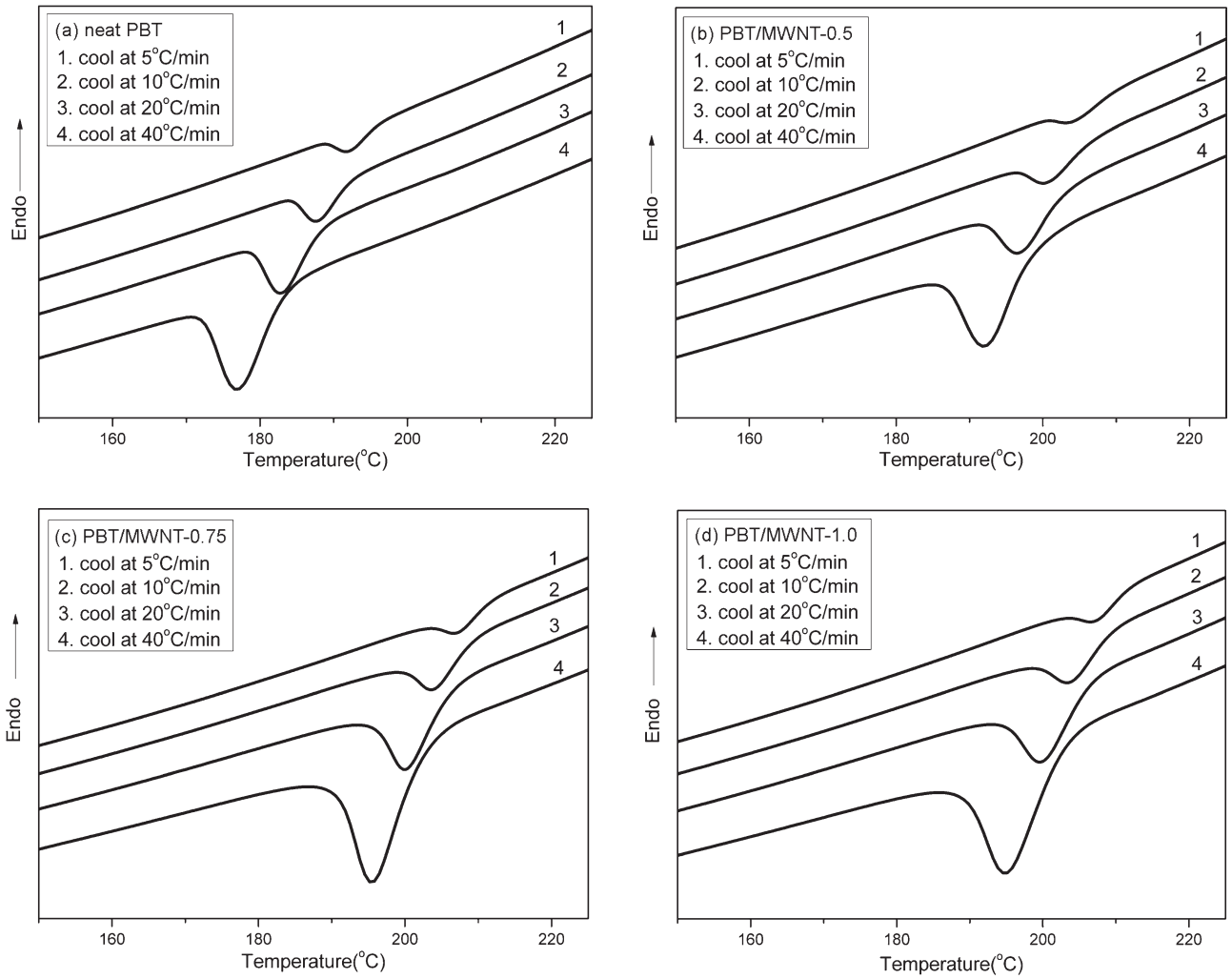

Figure 3. DSC curves of nonisothermal crystallization at different cooling rate: (a) neat PBT, (b) PBT/MWNT-0.5, (c) PBT/MWNT-0.75, and (d) PBT/MWNT-1.0.

the uniform molar ratio of monomer to initiator. However, the addition of MWNTs could considerably retard the process of the ring-opening polymerization; hence, the time of polymerization was set as 30 min to ensure completion.

Dispersion of MWNTs in the PBT Matrix

To investigate the effect of the MWNTs on the nonisothermal crystallization kinetics of PBT/MWNT nanocomposites, the dispersion of the MWNTs in the PBT matrix should be understood. Figure 1 shows the FESEM images of the PBT/MWNT nanocomposites. As illustrated, the white-dot regions represented the ends of MWNTs that were stretched out of the PBT matrix. The MWNTs exhibit good dispersion in the nanocomposites with 0.5 wt % and 0.75 wt % MWNT contents. However, with the content of MWNTs up to 1.0 wt %, some aggregation of MWNTs is observed, which is indicated in Figure 1(c) with arrow that signals a large bundle of MWNTs. More direct evidence about the dispersion of the MWNTs in the PBT matrix can be found from TEM images shown in Figure 2. It can be seen that most of the MWNTs are homogeneously nanodispersed in the PBT matrix, although some small entanglement is observed at high magnification.

Nonisothermal Crystallization Behavior

The nonisothermal crystallization exothermal curves of the neat PBT and the nanocomposites at various cooling rates are shown in Figure 3. The nonisothermal crystallization temperatures T_o (the onset temperature of crystallization), T_c (the end temperature of crystallization), T_p (the exothermic peak temperature of crystallization), and ΔH_c (the enthalpy for nonisothermal crystallization) are obtained from the curves and the results are listed in Table II. As the cooling rate increases, the T_o, T_c, and T_p shift to lower temperature, and the exotherms become broader. The results indicate that the crystallization occurs at lower temperature with faster cooling rates. At higher cooling rate, the molecular chains become less flexible and less mobile and have less time to diffuse into the crystallite lattice and to adjust and organize the chain configurations into more perfect crystallites. As a result, the extent of crystallite perfection also decreases with faster cooling rates.[26] On the contrary, at lower cooling rate, the PBT molecular chains may have enough time to pack up in a unit cell and then

Table II. Nonisothermal Parameters Determined from the DSC Exotherms for the Neat PBT and the PBT/MWNT Nanocomposites

Sample	ϕ (°C/min)	T_o (°C)	T_p (°C)	T_c (°C)	ΔH_c (J/g)	$t_{1/2}$(min)
neat PBT	5	196.5	192.2	188.2	11.1	1.97
	10	194.0	187.49	183.6	22.8	0.88
	20	190.5	182.8	177.7	45.9	0.54
	40	186.4	176.9	170.6	91.3	0.34
PBT/MWNT-0.5	5	209.5	204.2	199.9	10.5	1.34
	10	207.9	200.4	196.0	23.5	0.85
	20	205.5	196.6	190.7	46.2	0.53
	40	202.7	192.0	184.7	98.8	0.32
PBT/MWNT-0.75	5	212.6	207.0	202.8	11.8	1.26
	10	210.8	203.5	198.6	28.3	0.85
	20	209.1	199.8	193.0	61.4	0.54
	40	206.7	195.5	187.3	125.9	0.32
PBT/MWNT-1.0	5	212.8	207.0	202.5	11.7	1.32
	10	211.4	203.4	198.2	25.9	0.78
	20	209.2	199.5	192.3	55.8	0.46
	40	206.2	194.9	185.2	122.4	0.32

their nuclei grows up at higher temperature. Furthermore, the PBT/MWNT nanocomposites have higher T_p than the neat PBT at all cooling rates. Oburoğlu et al.[27] studied the crystallization behavior of PBT and PBT-based composites including 5 wt % of different types of filler, halloysite (tubular alumina-silicate as 1D filler), organo-montmorillonite (organically modified layered alumina-silicate as 2D filler), and calcite (spherical $CaCO_3$ particles as 3D filler). They found that 1D and 3D fillers acted as efficient nucleating agent and thus enhanced the crystallization rate of PBT, which was contributed to geometrically less efficient restriction effect of such fillers on the polymer chains, but 2D filler had considerably high surface area which could reduce the crystallization rate of PBT. Therefore, as for the PBT/MWNT nanocomposites, MWNTs as 1D fillers could promote the crystallization of PBT. However, with an increase in the MWNTs loadings, the dispersing degree of MWNTs declines and thus the efficiency of nucleation decreases. As for the ΔH_c, it can be seen that the values of all samples change slightly at the cooling rate of 5°C/min, but at the higher cooling rate, the values of the PBT/WMNT nanocomposites are larger than that of the neat PBT, which confirms that the incorporation of MWNTs promotes the crystallization of PBT.

The relative degree of crystllinity (X_t), as a function of crystallization temperature (T), is defined as:[28,29]

$$X_t = \frac{\int_{T_o}^{T} (dH_c/dT)dT}{\int_{T_o}^{T_c} (dH_c/dT)dT} \quad (4)$$

where dH_c/dT is the heat flow rate. T_o and T_c represent the onset and the end of crystallization temperature, respectively. In nonisothermal crystallization, the time t is related to the temperature T as

$$t = \frac{T_o - T}{\phi} \quad (5)$$

where T is the temperature at time t and the ϕ is the cooling rate. Figure 4 illustrates X_t as a function of t for the neat PBT and the PBT/MWNT nanocomposites at various cooling rate.

Another important parameter is the half-time of crystallization, $t_{1/2}$, which can be determined from Figure 4 and listed in Table II. In all cases, $t_{1/2}$ decreases with increasing the cooling rate, indicating that the crystallization at a higher cooling rate is faster than that at a lower cooling rate. And the $t_{1/2}$ values of the nanocomposites are smaller than that of the neat PBT, which implies that MWNTs act as heterogeneous nucleating agents to facilitate crystallization of PBT. Moreover, it can be seen that the $t_{1/2}$ value of PBT/MWNT-0.5 decreases magnificently by 32.0% at the cooling rate of 5°C/min, as compared with that of the neat PBT. However, in the case of direct melt compounding PBT with MWNTs,[23] the $t_{1/2}$ value of the nancompostie of PBT/MWNT containing 5 wt % MWNT content decreased by 17.7% at the same cooling rate. It suggests that PBT/MWNT nanocomposites have good dispersion of MWNTs via *in situ* method, and as a result, the MWNTs can dramatically enhance the crystallization rate even with low MWNT content. Additionally, as the content of MWNT increases from 0.5 wt % to 0.75 wt %, $t_{1/2}$ decreases gradually at the same cooling rate, which confirms the nucleation effect of MWNTs. However, as for the nanocomposite with 1.0 wt % MWNT content, such effect of MWNTs is slightly declined due to the aggregation of MWNTs in PBT matrix.

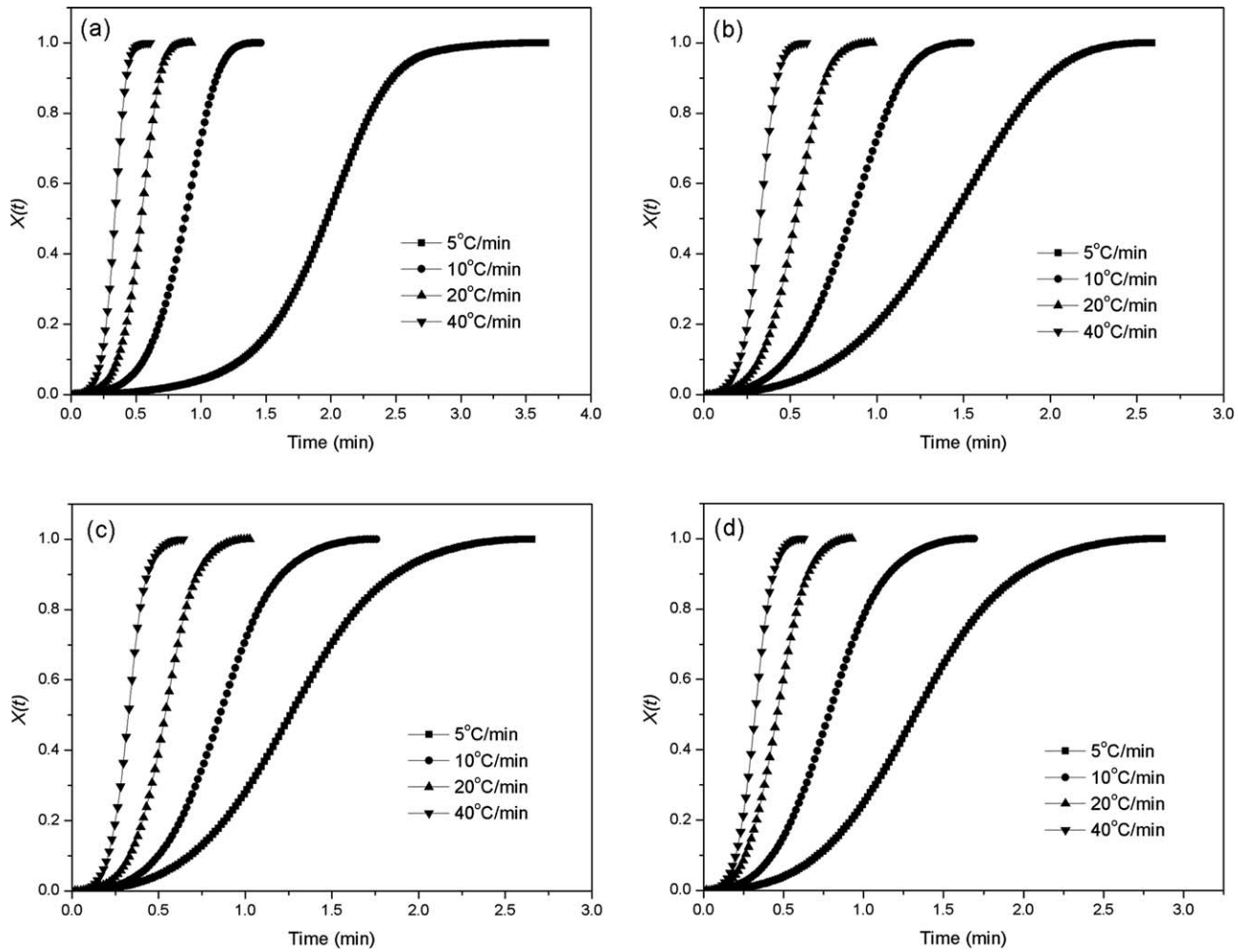

Figure 4. Relative crystallinity versus crystallization time for nonisothermal crystallization: (a) neat PBT, (b) PBT/MWNT-0.5, (c) PBT/MWNT-0.75, and (d) PBT/MWNT-1.0.

Nonisothermal Crystallization Kinetics

Modified Avrami Equation. It is well known that the Avrami equation[30,31] has been successfully used to describe isothermal crystallization behavior. Based on the assumption that the crystallization temperature is constant, the Avrami equation can explain the primary stage of nonisothermal crystallization behavior, as followed:

$$X(t)=1-\exp\left(-Z_t t^n\right) \tag{6}$$

The above equation can be transformed into its linear form:

$$\log\left[-\ln\left(1-X(t)\right)\right]=n\log t+\log Z_t \tag{7}$$

where n is the Avrami exponent related to the type of nucleation and to the geometry of growing crystals, and Z_t is the kinetic growth rate constant in the nonisothermal crystallization process. Considering the influence of various cooling rates on the nonisothermal crystallization process, Jeziorny[32] suggested that the rate parameter Z_t should be corrected as follows:

$$\log Z_c=\log Z_t/\phi \tag{8}$$

where Z_c is the modified crystallization rate constant with respect to the cooling rate ϕ.

Theoretically, plots of log [-ln(1-$X(t)$)] versus log t would be straight lines if eq. (7) adequately describes the nonisothermal crystallization behavior of a polymer, and the Avrami exponent n and Z_c are obtained from the slops and the intercepts, respectively. Plots of log $[-\ln(1-X(t))]$ versus log t for all samples are illustrated in Figure 5. As can be seen, there are some small deviations from linearity in the short-time region, which can be attributed to logarithmic plotting tending to exaggerate small errors in the assignment of the start of crystallization.[33] Furthermore, the linearity of the plots is poor, which indicates that the modified Avrami equation failed to describe satisfactorily the nonisothermal crystallization kinetics of the neat PBT and the PBT/MWNT nanocomposites. Despite this, the linear portion in the middle of the curves in Figure 5 is applied to determine n and Z_c, and the results are collected in Table III. It can be seen that with addition of MWNTs, the value of n increases evidently. This suggests the presence of MWNTs changes nucleation mechanism of PBT matrix. As known, the larger the value of Z_c, the higher the crystallization rate. For PBT and its nanocomposites, at the same cooling rate the Z_c values of the nanocomposites are higher than that of the neat PBT, which also

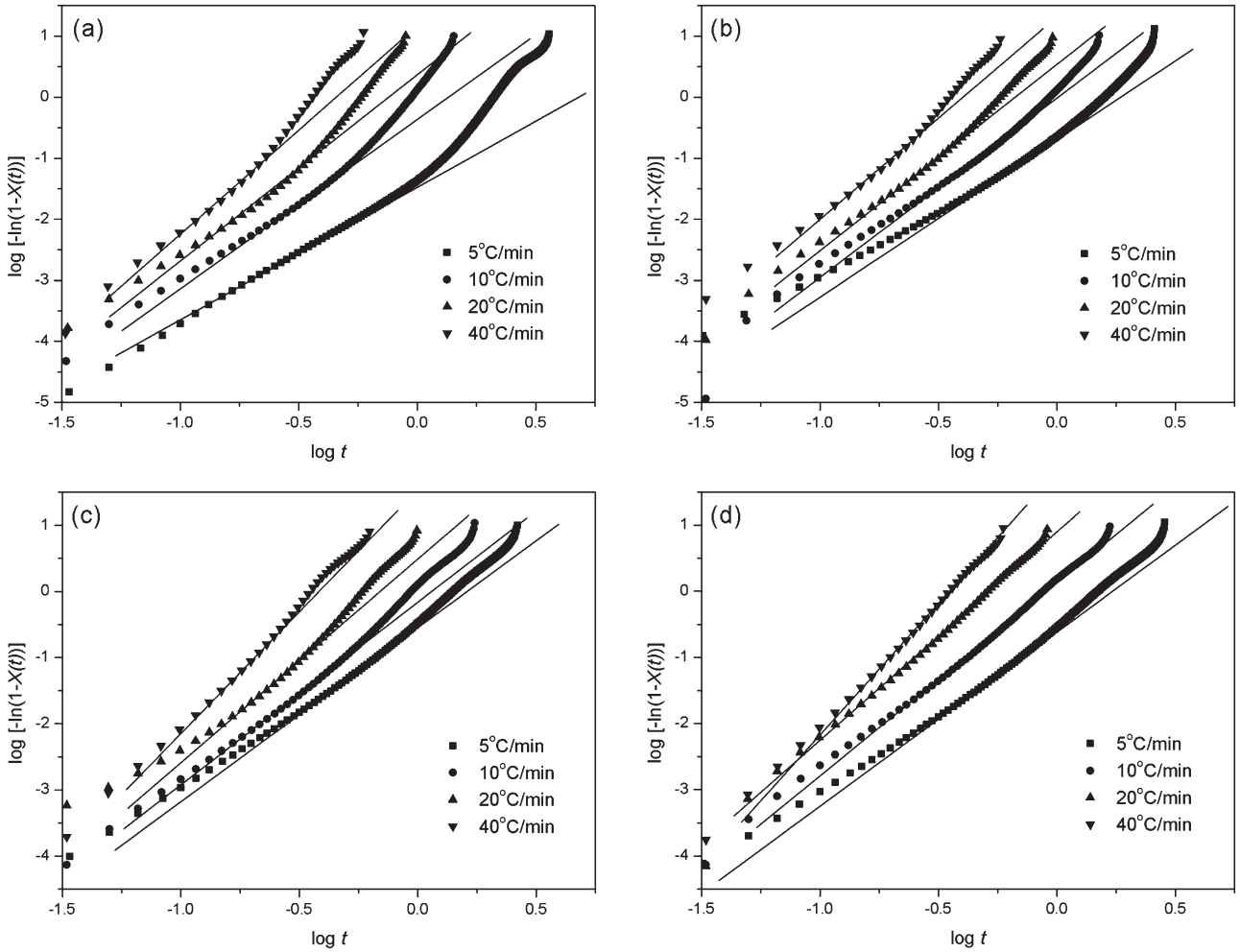

Figure 5. Plots of log[-ln(1-$X(t)$)] versus log$t$ for the modified Avrami equation at different cooling rate: (a) neat PBT, (b) PBT/MWNT-0.5, (c) PBT/MWNT-0.75, and (d) PBT/MWNT-1.0.

proves the enhancement of the crystallization rate of PBT due to the addition of MWNTs.

Ozawa Equation. Considering the influence of cooling rate on the nonisothermal crystallization, Ozawa[34] developed the Avrami model from the isothermal crystallization to the nonisothermal case by presuming that crystallization occurs at a constant cooling rate, and modified the Avrami equation as follows:

$$X(T)=1-\exp\left[-K(T)/\phi^{m}\right] \tag{9}$$

where ϕ is the cooling rate, $X(T)$ is the relative crystallinity, $K(T)$ is the cooling crystallization function and m is the Ozawa exponent depending on the dimension of crystal growth. From equation (9), it follows:

$$\log\left[-\ln\left(1-X(T)\right)\right]=\log K(T)-m\log\phi \tag{10}$$

Figure 6 illustrates the Ozawa plots of log[-ln(1-$X(T)$)] against $\log\phi$ at various temperatures for the neat PBT and the PBT/MWNT nanocomposites. If the Ozawa model correctly describes the nonisothermal crystallization kinetics of samples, plots of log [-ln(1-$X(T)$)] against $\log\phi$ should create a straight lines and kinetic paramenters $K(T)$ and m could be obtained from the intercepts and slopes of the lines, respectively. However, for all of the samples, clearly no straight lines are obtained, indicating the failure of Ozawa model to describe the nonisothermal crystallization kinetics of PBT and its nanocomposites. It is well known that the Ozawa model is based on the quasi-isothermal crystallization. Under nonisothermal crystallization, the crystallization rate is no longer constant but a function of both time and cooling rate. Moreover, other effects such as the slow secondary crystallization and the folded chain length are also not considered in the Ozawa model[35].

Combined Avrami/Ozawa Equation. To overcome the shortcomings of the above models, Mo and Liu[36] proposed a new kinetic model of nonisothermal crystallization by combining the Avrami and Ozawa models:

$$\log Z_t+n\log t=\log K(T)-m\log\phi \tag{11}$$

$$\log\phi=\log F(T)-\alpha\log t \tag{12}$$

where the parameters of $F(T)$ and α are equal to $[K(T)/Z_t]^{1/m}$ and n/m, respectively. The physical meaning of the $F(T)$ is the necessary value of cooling rate approaching to the degree of crystallinity at unit crystallization time,[37] and α is the ratio between the Avrami and Ozawa exponents. The smaller the

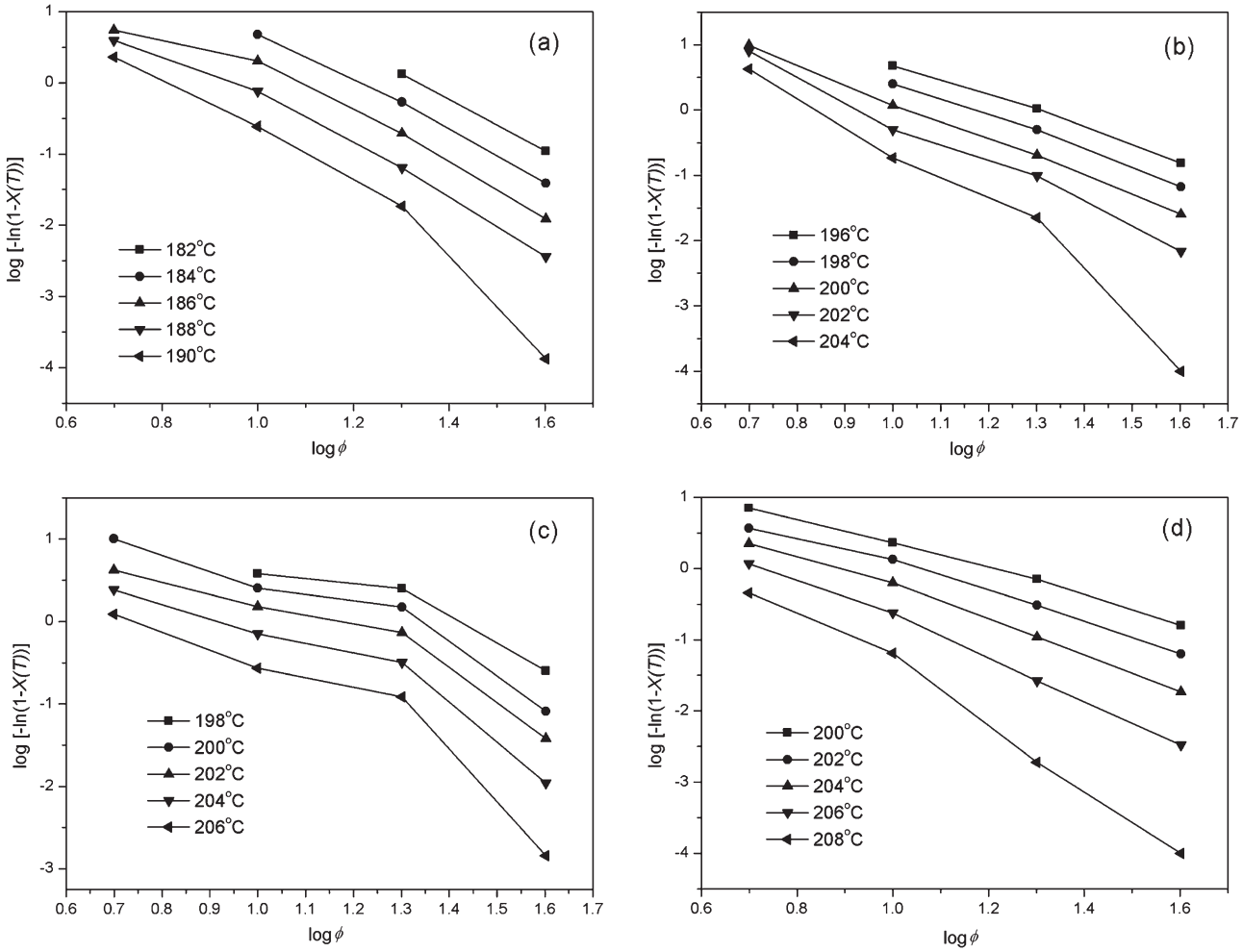

Figure 6. Plots of log[-ln(1-$X(T)$)] versus log φ for the Ozawa equation at different temperature: (a) neat PBT, (b) PBT/MWNT-0.5, (c) PBT/MWNT-0.75, and (d) PBT/MWNT-1.0.

value of $F(T)$, the higher the crystallization rate becomes. According to the eq. (12), plotting log ϕ versus log t at a given relative degree of crystallinity can generate a straight line, as shown in Figure 7. The kinetic parameters of $F(T)$ and α can be obtained from the intercept and slope of the plots.

As can be seen in Figure 7, all of the plots exhibite a good linear relationship (See the regression coefficient, *RC*, in Table III), which confirms the validity of the combined Avrami/Ozawa equation in the case of nonisothermal crystallization. The values of $F(T)$ and α are listed in Table III. On one hand, for all of the samples, the values of $F(T)$ increase with the increasing relative crystallinity, suggesting that the required cooling rate should be higher in order to achieve the higher degree of crystallinity at unit crystallization time. On the other hand, the values of $F(T)$ depend on the MWNTs content. As for neat PBT, PBT/MWNT-0.5 and PBT/MWNT-0.75, with increasing the content of MWNTs, the values of $F(T)$ decline at the same relative degree of crystallinity, indicating that the more MWNTs loaded the faster the crystallization rate becomes. However, the values of $F(T)$ for PBT/MWNT-1.0 slightly increases, compared with that for PBT/MWNT-0.75, which is in accord with the tendency of $t_{1/2}$. In addition, comparing with the α values of the neat PBT and the nanocomposites, it is found that the α values of the later is higher than that of the former. Considering that α is equal to n/m, the higher value of α means the effect of MWNTs on the nucleation type of PBT is more notable than that on the growth dimension. This probably implies that the presence of MWNTs makes the nucleation process of PBT change from homogeneous to heterogeneous.

Crystallization Activation Energy. As for the nonisothermal crystallization at different cooling rates, Kissinger[38] proposed a method for determining the activation energy, ΔE, for the transport of the macromolecular segments to the growing surface:

$$\frac{d[\ln(\phi/T_p^2)]}{d(1/T_p)} = \frac{-\Delta E}{R} \tag{13}$$

where R is the gas contant, ϕ is the cooling rate and T_p is the crystallization peak temperature. Accordingly, the crystallization activation energy could be determined from the slope of the plot of $\ln(\phi/T_p^2)$ versus $1/T_p$, as shown in Figure 8 and Table IV. It can be seen that the ΔE values of the nanocomposites are

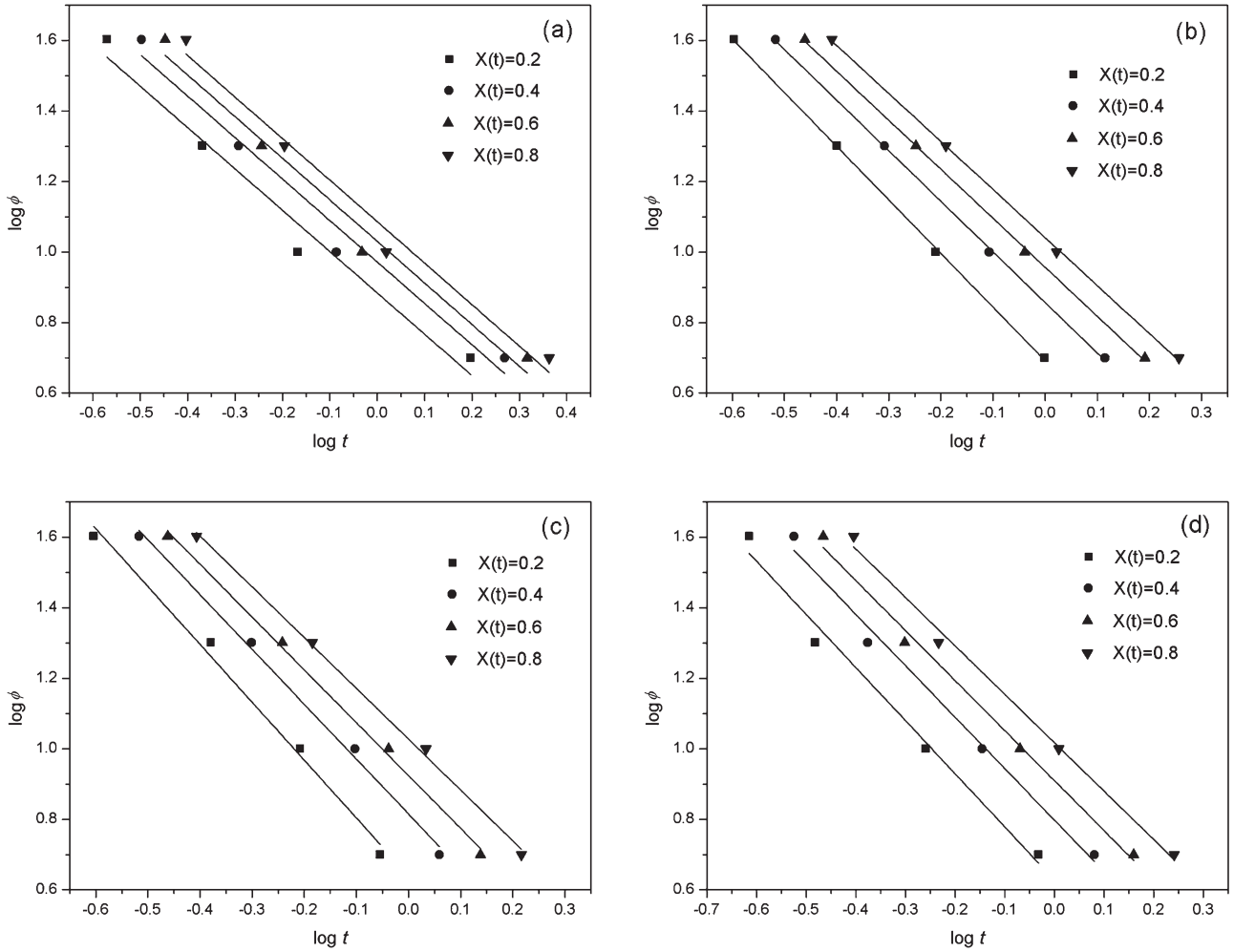

Figure 7. Plots of $\log \varphi$ versus $\log t$ for the combined Avrami/Ozawa equation at different degrees of crystallinity: (a) neat PBT, (b) PBT/MWNT-0.5, (c) PBT/MWNT-0.75, and (d) PBT/MWNT-1.0.

Table III. Nonisothermal Crystallization Kinetics Parameters About the Modified Avrami Model and the Combined Avrami/Ozawa Model for the Neat PBT and the PBT/MWNT Nanocomposites

	Modified Avrami equation				Combined Avrami/Ozawa equation			
Samples	ϕ (°C/min)	Z_t (min^{-1})	n	Z_c (min^{-1})	$X(T)$%	$F(T)$	α	RC
neat PBT	5	0.037	2.234	0.519	20	7.661	1.172	0.963
	10	0.255	2.386	0.872	40	9.376	1.176	0.969
	20	0.719	2.433	0.984	60	10.723	1.180	0.971
	40	4.764	2.882	1.040	80	12.202	1.178	0.975
PBT/ MWNT-0.5	5	0.175	2.243	0.706	20	4.920	1.521	0.999
	10	0.637	2.539	0.956	40	7.198	1.435	0.999
	20	2.056	2.690	1.037	60	9.059	1.390	0.999
	40	8.453	2.851	1.055	80	10.999	1.362	0.999
PBT/MWNT-0.75	5	0.340	2.951	0.806	20	4.362	1.641	0.988
	10	1.130	3.357	1.012	40	6.540	1.555	0.994
	20	6.637	3.718	1.099	60	8.399	1.498	0.996
	40	59.156	3.994	1.107	80	10.651	1.440	0.997
PBT/MWNT-1.0	5	0.215	2.413	0.735	20	4.379	1.507	0.980
	10	0.887	2.596	0.988	40	6.588	1.459	0.987
	20	4.989	2.899	1.083	60	8.533	1.419	0.991
	40	25.119	3.438	1.084	80	10.716	1.374	0.992

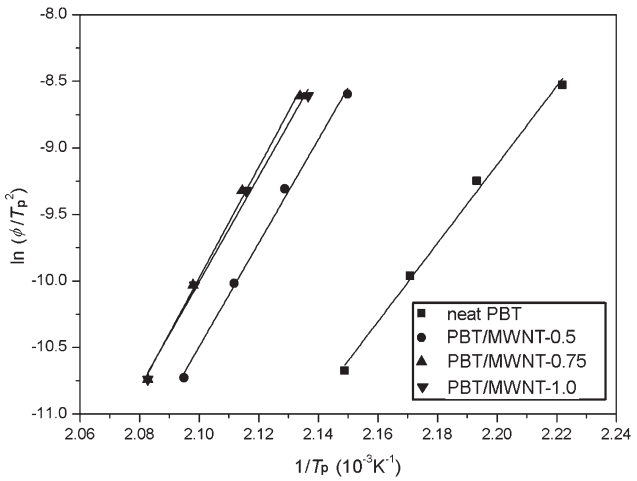

Figure 8. Kissinger plots of $\ln(\phi/T_p^2)$ versus $1/T_p$ for the neat PBT and the PBT/MWNT nanocomposites.

higher than that of the neat PBT, which is also observed in PBT/calcite composites[27] and PBT/halloysite composites,[27,39] suggesting a more difficult motion of the PBT chain segments in composites. Obviously, the presence of MWNTs could not only promote crystallization of PBT as a nucleating agent but also retard crystallization as a physical hindrance. However, combined with the above results, it can be found that the nucleation effect of MWNTs plays a dominant role in crystallization process of PBT.

CONCLUSION

In this study, PBT/MWNT nanocomposites were prepared by *in situ* ring-opening polymerization of CBT. FESEM and TEM revealed that the MWNTs have good dispersion in the PBT matrix as the MWNT contents were 0.5 wt % and 0.75 wt %. The nonisothermal crystallization kinetics of the neat PBT and the PBT/MWNT nanocomposites was investigated by the DSC technique. Three different models have been used to analyze the crystallization of all samples. Compared with the modified Avrami equation and the Ozawa equation, the combined Avrami/Ozawa equation provided a satisfactory description of the crystallization processes for PBT and its nanocomposites. Moreover, the MWNTs acted as nucleating agent greatly increasing crystallization rate of nanocomposites, which could be confirmed by the parameters of $t_{1/2}$, n, Z_c, and $F(T)$. Nevertheless, the crystallization activation energies of PBT and its nanocomposites indicated that the incorporation of MWNT hindered the mobility of the PBT chain segments.

Table IV. Crystallization Activation Energies of the Neat PBT and the PBT/MWNT Nanocomposites

Sample	ΔE(kJ/mol)
neat PBT	245.11
PBT/MWNT-0.5	323.64
PBT/MWNT-0.75	346.38
PBT/MWNT-1.0	328.75

ACKNOWLEDGMENTS

The authors gratefully acknowledge the financial support from the Natural Science Foundation of Fujian Province, China (No. 2013J01167) and the Research Foundation of Education Bureau of Fujian Province, China (No. JK2013031).

REFERENCES

1. Mark, J. E. Polymer Data Handbook; Iroh, J. O., Ed.; Oxford University Press: New York, **1999**; p 349.
2. Iijima, S. *Nature* **1991**, *354*, 56.
3. Nogales, A.; Broza, G.; Roslaniec, Z.; Schulte, K.; Sics, I.; Haiao, B. S.; Sanz, A.; Garcia-Gutierrez, M. C.; Rueda, D. R.; Domingo, C.; Ezquerra, T. A. *Macromolecules* **2004**, *37*, 7669.
4. Broza, G.; Kwiatkowska, M.; Roslaniec, Z.; Schulte, K. *Polymer* **2005**, *46*, 5860.
5. García-Gutiérrez, M. C.; Nogales, A.; Rueda, D. R.; Domingo, C.; Garcia-Ramos, J. V.; Broza, G.; Roslaniec, Z.; Schulte, K.; Ezquerra, T. A. *Compos. Sci. Technol.* **2007**, *67*, 798.
6. Wu, D.; Wu, L.; Zhang, M. *J. Polym. Sci. Part B: Polym. Phys.* **2007**, *45*, 2239.
7. Shao, W.; Wang, Q.; Wang, F.; Chen, Y. *Carbon* **2006**, *44*, 2708.
8. McCarthy, B.; Coleman, J. N.; Czerw, R.; Dalton, A. B.; in het Panhuis, M.; Maiti, A.; Drury, A.; Bernier, P.; Nagy, J. B.; Byrne, H. J.; Carroll, D. J.; Blau, W. J. *J. Phys. Chem. B* **2002**, *106*, 2210.
9. Qu, L.; Veca, L. M.; Lin, Y.; Kitaygorodskiy, A.; Chen, B.; McCall, A. M.; Connell, J. W.; Sun, Y. P. *Macromolecules* **2005**, *38*, 10328.
10. Frizzell, C. J.; in het Panhuis, M.; Coutinho, D. H.; Balkus, Jr K. J.; Minett, A. I.; Blau, W. J.; Coleman, J. N. *Phys. Rev. B* **2005**, *72*, 245420.
11. Hughes, M.; Chen, G. Z.; Schaffer, M. S. P.; Fray, D. J.; Windle, A. H. *Chem. Mater.* **2002**, *14*, 1610.
12. Grossiord, N.; Loos, J.; Koning, C. E. *J. Mater. Chem.* **2005**, *15*, 2349.
13. Miltner, H. E.; Grossiord, N.; Lu, K.; Loos, J.; Koning, C. E.; Mele, B.V. *Macromolecules* **2008**, *41*, 5753.
14. Saligheh, O.; Arasteh, R.; Forouharshad, M.; Eslami-Farsani, R. *J. Macromol. Sci. Part B: Phys.* **2011**, *50*, 1031.
15. Saligheh, O.; Forouharshad, M.; Arasteh, R.; Eslami-Farsani, R.; Khajavi, R.; Yadollah Roudbari, B. *J. Polym. Res.* **2013**, *20*, 65.
16. Saeed, K.; Khan, I. *Iran. Polym. J.* **2014**, *23*, 53.
17. Cochet, M.; Maser, W. K.; Benito, A. M.; Callejas, M. A.; Martinez, M. T.; Benoit, J. M.; Schreiber, J.; Chauvet, O. *Chem. Commun.* **2001**, 1450.
18. Sainz, R.; Benito, A. M.; Martinez, M. T.; Galindo, J. F.; Sotres, J.; Baro, A. M.; Corraze, B.; Chauvet, O.; Maser, W. K. *Adv. Mater.* **2005**, *17*, 278.

19. in het Panhuis, M.; Sainz, R.; Innis, P. C.; Kane-Maguire, L. A. P.; Benito, A. M.; Martínez, M. T.; Moulton, S. E.; Wallace, G. G.; Maser, W. K. *J. Phys. Chem. B* **2005**, *109*, 22725.
20. Romhány, G.; Vígh, J. Thomann, R. Karger-Kocsis, J. Sajó, I. E. *Macromol. Mater. Eng.* **2011**, *296*, 544.
21. Wu, F.; Yang, G. *Polym. Adv. Technol.* **2010**, *22*, 1466.
22. Wu, F.; Yang, G. *J. Appl. Polym. Sci.* **2010**, *118*, 2929.
23. Wu, D.; Wu, L.; Yu, G.; Xu, B.; Zhang, M. *Polym. Eng. Sci.* **2008**, *48*, 1057.
24. Borman, W. F. H. *J. Appl. Polym. Sci.* **1978**, *22*, 2119.
25. Solomon, O. F.; Ciutâ, I. Z. *J. Appl. Polym. Sci.* **1962**, *6*, 683.
26. Wu, D.; Zhou, C.; Fan, X.; Mao, D.; Bian, Z. *J. Appl. Polym. Sci.* **2006**, *99*, 3257.
27. Oburoğlu, N.; Ercan, N.; Durmus, A.; Kaşgöz, A. *J. Appl. Polym. Sci.* **2012**, *123*, 77.
28. Hay, J. N.; Sabir, M. *Polymer* **1969**, *10*, 203.
29. Hay, J. N.; Fitzgerald, P. A.; Wiles, M. *Polymer* **1976**, *17*, 1015.
30. Avrami, M. *J. Chem. Phys.* **1939**, *7*, 1103.
31. Avrami, M. *J. Chem. Phys.* **1940**, *8*, 212.
32. Jeziorny, A. *Polymer* **1978**, *19*, 1142.
33. Seo, Y.; Kim, J.; Kim, K. U.; Kim, Y. C. *Polymer* **2000**, *41*, 2639.
34. Ozawa, T. *Polymer* **1971**, *12*, 150.
35. Kuo, M. C.; Huang, J. C.; Chen, M. *Mat. Chem. Phys.* **2006**, *99*, 258.
36. Liu, T.; Mo, Z.; Wang, S.; Zhang, H. *Polym. Eng. Sci.* **1997**, *37*, 568.
37. Weng, W.; Chen, G.; Wu, D. *Polymer* **2003**, *44*, 8119.
38. Kissinger, H. E. *Anal. Chem.* **1957**, *29*, 1702.
39. Oburoğlu, N.; Ercan, N.; Durmus, A.; Kaşgöz, A. *J. Macromol. Sci. Part B: Phys.* **2012**, *51*, 860.